www.czasopisma.pan.pl PAN POLSKA AKADEMIA NAUK www.journals.pan.pl

ARCHIVES OF ACOUSTICS Online First August 19, 2024 doi: 10.24425/aoa.2024.148807

Research Paper

Mutually Orthogonal Complementary Golay Coded Sequences: An In-vivo Study

Ihor TROTS*, Jurij TASINKIEWICZ, Andrzej NOWICKI

Department of Ultrasound, Institute of Fundamental Technological Research
Polish Academy of Sciences
Warsaw, Poland

*Corresponding Author e-mail: igortr@ippt.pan.pl

(*received April 22, 2024; accepted July 26, 2024; published online August 19, 2024*)

Fast and high-quality ultrasound imaging allows to increase the effectiveness of detecting tissue changes at the initial stage of disease. The aim of the study was to assess the quality of ultrasound imaging using mutually orthogonal, complementary Golay coded sequences (MOCGCS). Two 16-bits MOCGCS sets were implemented in the Verasonics Vantage™ scanner. Echoes from a perfect reflector, a custom-made nylon wire phantom, a tissue-mimicking phantom, and in-vivo scans of abdominal aorta and common carotid artery were recorded. Three parameters of the detected MOCGCS echoes: signal-to-noise ratio (SNR), side-lobe level (SLL), and axial resolution were evaluated and compared to the same parameters of the echoes recorded using standard complementary Golay sequences (CGS) and a short, one sine cycle pulse. The results revealed that MOCGCS transmission maintained comparable echo quality metrics (SNR, SLL, and axial resolution) compared to CGS and short pulses. Notably, both MOCGCS and CGS offered similar SNR improvements (5 dB–9 dB) in comparison to the short pulse for wires placed at depths up to 8 cm. Analysis of axial resolution, estimated at the full width at half maximum level, revealed near-identical values for all transmitted signals (0.17 μs for MOCGCS, 0.16 μs for CGS, and 0.18 μs for short pulse). MOCGCS implementation in ultrasound imaging offers the potential to significantly reduce image reconstruction time while maintaining image quality comparable to CGS sequences. In the experimental study we have shown that MOCGCS offers advantages over conventional CGS by enabling two times faster data acquisition and image reconstruction without compromising image quality.

Keywords: coded excitation; Golay codes; synthetic aperture; ultrasound imaging.

1. Introduction

Modern ultrasound diagnostics require exceptional image quality, characterized by deep penetration depth, high signal-to-noise ratio (SNR), and excellent resolution. However, achieving this trade-off between penetration and resolution necessitates alternative approaches. Wide-band coded sequences, combined with echo compression techniques, offer a promising solution (NOWICKI *et al.*, 2003). These sequences allow for increased SNR and deeper visualization without exceeding power limitations, even enabling the use of higher frequencies. Among the various coded sequences explored in ultrasound, Golay codes have emerged as frontrunners (GOLAY, 1961). Their unique ability to suppress side lobes in the transmitted signal makes them particularly attractive. This property minimizes interference and improves overall signal quality.

While computational capabilities play a role, a crucial factor limiting the frame rate (images per second) in ultrasound imaging is the speed of data acquisition. This speed depends on the sound wave velocity in the target tissue, imaging depth, and the number of scanned lines.

A promising approach to overcome this limitation involves transmitting multiple scanning signals simultaneously. However, separating the resulting echoes requires the transmitted signals to be orthogonal, minimizing interference. Fortunately, specific pairs of Golay coded sequences, known as MOCGCS, possess this desired property (BAE, 2003).

MOCGCS have attracted significant research interest in recent years due to their potential applications in various fields, including ultrasound (Gran, Jensen, 2006; Demi *et al.*, 2013; Trots *et al.*, 2004; 2011; Wu *et al.*, 2020; Tian *et al.*, 2021). Their key advantage lies in the orthogonality property, enabling significant increases in data acquisition rate and consequently, faster image reconstruction (frame rate). While prior studies explored using MOCGCS for 2D B-mode image reconstruction by comparing simultaneous transmission with short pulse approaches (Chiao, Thomas, 2000; Bae *et al.*, 2002; Kim, Song, 2003; Misaridis, Jensen, 2005; Peng *et al.*, 2006; Ramalli *et al.*, 2015; Zhao, Luo, 2018; Kumru, Koymen, 2018), a critical gap remains. No research has conducted an in-depth analysis of how MOCGCS echoes behave in real-world scenarios, particularly regarding the effectiveness of matched filtering for echo separation.

This paper addresses this gap by experimentally evaluating the feasibility of MOCGCS in ultrasound diagnostics. We analyze and compare echoes acquired using MOCGCS with those obtained from conventional complementary Golay sequences (CGS) and short pulses. Our analysis focuses on echoes from various targets, including a brass plate, a custom-made nylon wire phantom, and a tissue-mimicking phantom. Specifically, we compare signal parameters such as pulse duration, side-lobe level (SLL), and SNR for each excitation signal. Matched filtering is employed for MOCGCS and CGS emissions to separate echoes and suppress side-lobes. These parameters include pulse duration at the −6 dB and −20 dB levels, signal SLL, and SNR. In the case of MOCGCS and CGS emissions, matched filters were used to separate the echoes and suppress the signal side-lobes. The experimental setup utilizes a commercially available ultrasound system (Verasonics Vantage™) equipped with a 128-element linear array transducer.

2. Materials and methods

The experiment utilized a Verasonics Vantage™ research ultrasound system equipped with a 128-element linear array transducer (L7-4), operating at a center frequency of 5.2 MHz with a bandwidth of 60 %. Three types of signals were generated for transmission:

- a conventional 16-bit complementary Golay sequence (CGS) pair,
- two 16-bit, mutually orthogonal complementary Golay code sets (MOCGCS),
- a one sine cycle pulse (short pulse) with a nominal frequency of 5.2 MHz.

Ultrasound echoes were collected using three different targets immersed in a water tank:

- perfect reflector: this initial measurement with a perfect reflector allowed us to estimate the compressed pulse duration for each signal type (MOCGCS, CGS, and short pulse),
- custom-made wire phantom: a phantom consisting of fine nylon wires (diameter 0.25 mm) arranged vertically with 20 mm axial spacing was used to compare the side-lobe level (SLL) for different excitation signals,
- tissue-mimicking phantom: this phantom with an attenuation of 0.5 dB/(MHz·cm) facilitated the comparison of signal-to-noise ratio (SNR) across different signals.

The basic algorithm of MOCGCS compression is given below. Consider two L-bit long codes G_{1i} and G_{2i}, $i = 1, 2, ..., M$, that are complementary pairs (G_{11} and G_{12} is a complementary pair #1, and G_{21} and G_{22} is a complementary pair #2) and obey the following condition (Trots, 2015; Trots *et al.*, 2015):

$$R_{G_{11}}(n) + R_{G_{12}}(n) = \begin{cases} 2L, & n = 0, \\ 0, & n \neq 0, \end{cases}$$
$$R_{G_{21}}(n) + R_{G_{22}}(n) = \begin{cases} 2L, & n = 0, \\ 0, & n \neq 0, \end{cases} \tag{1}$$

where the autocorrelation function R of the coded sequence in Eq. (1) is defined as follows (Misaridis, 2001):

$$R(n) = \begin{cases} \sum_{k=0}^{L-1-n} C(k)C(k-n), & n = 0, ..., L-1, \\ R(-n), & n = -(L-1), ..., -1, \end{cases} \tag{2}$$

where $C(k)$, $k = 0, ..., L-1$ denote the coded sequence G_{1i}, G_{2i}, $i = 1, 2$ of the length L.

Two pairs of Golay codes CGC, G_{1i} and G_{2i}, are said to be mutually orthogonal, or MOCGCS pairs, if the sum of their cross-correlation functions is zero:

$$\sum_{i,j=1}^{2} R_{G_{1i}G_{2j}} = 0. \tag{3}$$

The cross-correlation functions in Eq. (3) are defined as follows (Tseng, Liu, 1972):

$$R_{G_{1i}G_{2j}}(n) = \begin{cases} \sum_{k=0}^{L-1-n} G_{1i}(k)\, G_{2j}(k-n), \\ \qquad n = 0, ..., L-1, \\ \sum_{k=0}^{L-1-n} G_{1i}(k-n)\, G_{2j}(k), \\ \qquad n = -(L-1), ..., -1. \end{cases} \tag{4}$$

Thus, the CGC pairs G_{1i} and G_{2i}, $i = 1, 2$, form a MOCGCS set if they satisfy Eqs. (1) and (3) simultaneously. The key benefit of MOCGCS, as defined by Eq. (3), lies in their ability to enable the simultaneous transmission of two CGS pairs without interference during reception, allowing for the separation of individual echoes.

In this work, two sets of MOCGCS – orthogonal sets of $\{G_1, G_2\}$ – are used:

$$G_{11} = [-1\ -1\ -1\ 1\ -1\ -1\ 1\ -1\ -1\ -1\ -1\ 1\ 1\ 1\ -1\ 1],$$

$$G_{12} = [-1\ 1\ -1\ -1\ -1\ 1\ 1\ 1\ -1\ 1\ -1\ -1\ 1\ -1\ -1\ -1],$$

$$G_{21} = [-1\ -1\ -1\ 1\ -1\ -1\ 1\ -1\ 1\ 1\ 1\ -1\ -1\ -1\ 1\ -1],$$

$$G_{22} = [-1\ 1\ -1\ -1\ -1\ 1\ 1\ 1\ 1\ -1\ 1\ 1\ -1\ 1\ 1\ 1].$$

Assuming orthogonal Golay sequences of length $L = 16$ bits, the two code sequences $\{G_{1i}, G_{2i}\}$ are transmitted by two transducer elements (namely, #1 and #2). First, the orthogonal signals $\{G_{11}, G_{21}\}$ are transmitted. Then, the corresponding echoes are detected and stored for further processing. Next, the process is repeated for the second pair of orthogonal signals $\{G_{12}, G_{22}\}$. The detected signals, which are a superposition of echoes corresponding to $\{G_{1i}, G_{2i}\}$, can be compressed by summing the correlation functions of each received sequence with the sequence transmitted by the same transducer element. For example, to recover the echo for transducer element #1 (i.e., the pair G_{1i} that was transmitted by transducer element #1), for the first and second transmissions, one should compute the sum of cross-correlation functions P_{G_1} of the received signals $R_{S_iG_{1i}}$ with the corresponding transmitted codes G_{1i}, $i = 1, 2$, using Eq. (4) as follows:

$$P_{G_1} = \sum_{i=1}^{2} R_{S_iG_{1i}}. \tag{5}$$

Figure 1 illustrates the data acquisition scheme for MOCGCS transmission. Two sets of MOCGCS codes, denoted as G_{1i} and G_{2i}, were transmitted simultaneously using two adjacent elements of the linear array transducer. During the first transmission, element #1 transmitted code G_{11} while element #2 transmitted code G_{21}. This pattern was reversed for the second transmission, with element #1 transmitting G_{12} and element #2 transmitting G_{22}. In both transmissions, echoes were acquired by all transducer elements simultaneously. For comparison, CGS transmission involved transmitting only one complementary pair (G_{11} and G_{12}) by the same elements (#1 and #2) during two consecutive transmissions. Similarly, the short pulse was transmitted and received by elements #1 and #2, implementing a synthetic transmit aperture (STA) with a 2-element sub-aperture in transmit mode and a 2-element stride. This STA scheme was used throughout the experimental measurements (detailed in Sec. 3).

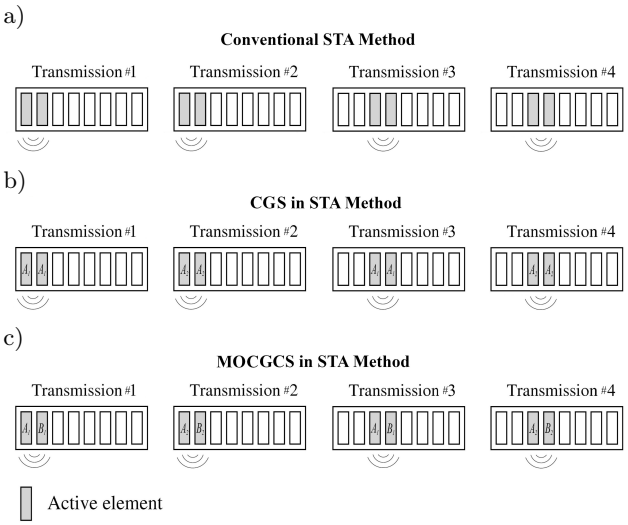

Fig. 1. Data acquisition scheme for: a) short pulse; b) CGS; c) MOGCS transmission in a 2-element synthetic transmit aperture method with a 2-elements stride. In all three configurations, all elements of the array are active.

Raw data were collected at a sampling rate of 20.8 MHz and stored for further processing. The processing methods differed based on the transmitted signal type:

- MOCGCS echoes: processing followed the method described in (Trots *et al.*, 2022),
- CGS echoes: a conventional matched filtering technique (Misaridis, 2001) was employed to compress the signals and suppress side-lobes.

All signal processing algorithms were implemented in MATLAB®.

3. Results

Figure 2 presents the radio frequency (RF) signals detected from a perfect reflector (brass plate) for different transmitted signals at a 5.2 MHz center frequency:

- Fig. 2a: echo for one cycle short pulse,
- Figs. 2b and 2c: MOCGCS echoes, representing the superposition of 16-bit codes G_{11} and G_{21}, and G_{12} and G_{22}, respectively, transmitted simultaneously by elements #1 and #2,
- Figs. 2d and 2e: CGS echoes resulting from single transmissions of codes G_{11} and G_{12} by elements #1 and #2. Elements #1 and #2 were used for transmission, and element #1 received the echoes. All coded sequences were 16 bits long, and the overall bandwidth was about 60 %.

Figure 3 depicts the envelopes of the signals reflected from a brass plate (corresponding RF echoes shown in Fig. 2). For MOCGCS and CGS signals, matched filtering was applied to compress the RF echoes before envelope detection. Figure 3 shows only the G_1 code envelope from the MOCGCS transmission. The same code $G_1 = \{G_{11}, G_{12}\}$ was used as the CGS example in Figs. 2d and 2e.

The half-maximum durations (measured at −6 dB) of the envelopes for both MOCGCS and CGS were nearly identical, at approximately 0.17 μs and 0.16 μs, respectively. The corresponding value for the short

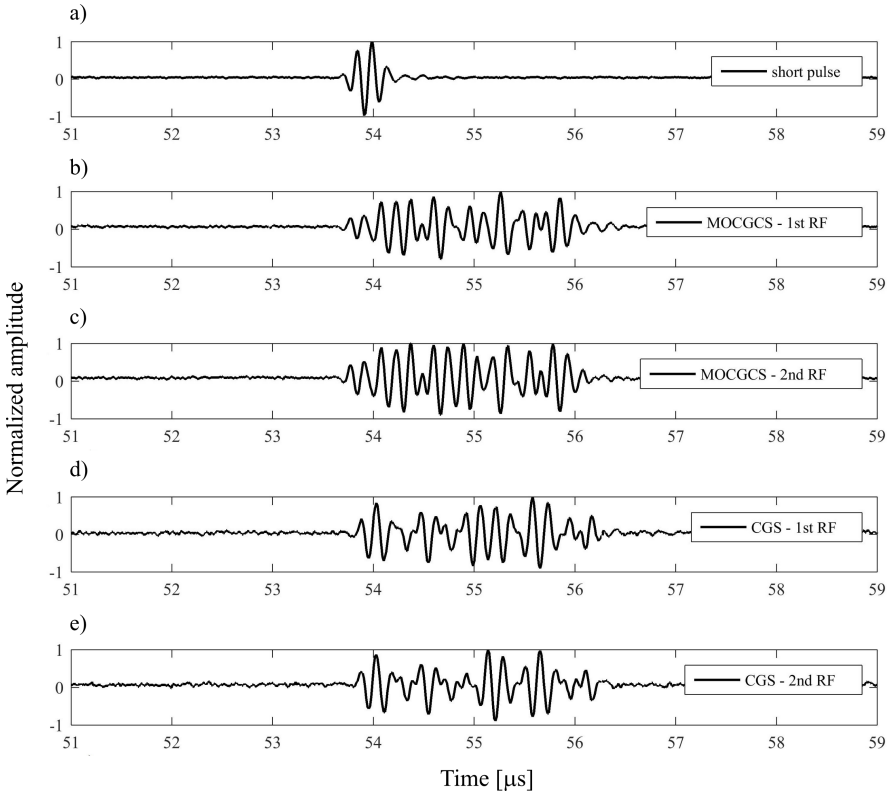

Fig. 2. RF echo signal from a perfect reflector for: a) short pulse transmission; b) MOCGCS echo being a superposition of codes G_{11} and G_{21}; c) MOCGCS echo being a superposition of codes G_{12} and G_{22}; d) CGS echo resulting from G_{11} sequence transmitted; e) CGS echo resulting from G_{12} sequence transmitted. Elements #1 and #2 were used in TX mode; the echoes were detected by element #1.

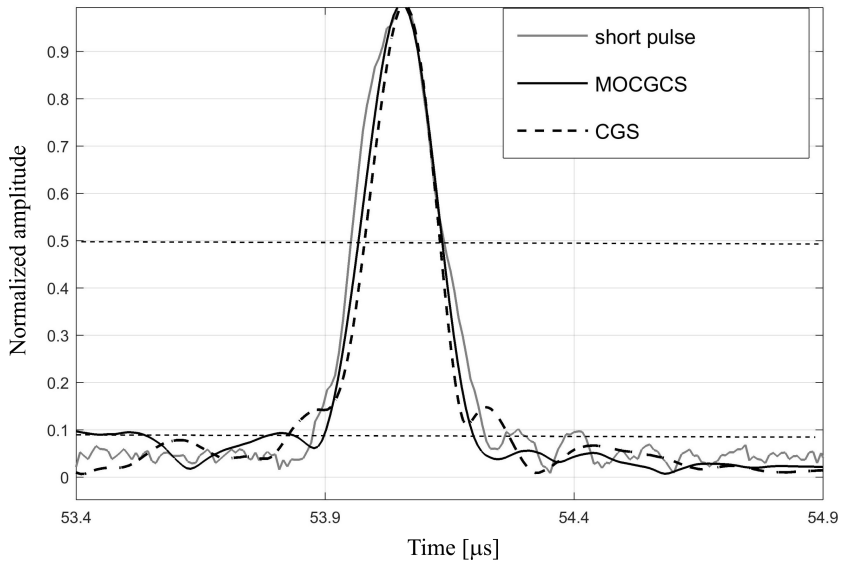

Fig. 3. Envelopes of the processed RF echoes obtained from the perfect reflector using the short pulse, the MOCGCS and the CGS transmitted signals.

pulse was slightly higher at 0.18 μs. Translating these time durations to spatial distance using the ultrasound speed provides axial resolutions of approximately 0.52 mm and 0.49 mm for MOCGCS and CGS, respectively. The short pulse resulted in a slightly lower resolution of 0.55 mm.

The envelope durations at the −20 dB level were 0.30 μs for MOCGCS, 0.36 μs for CGS, and 0.35 μs for the short pulse transmission. These durations translate to spatial resolutions of 0.92 mm for MOCGCS, 1.11 mm for CGS, and 1.08 mm for the short pulse.

In Fig. 4, the envelopes of the RF signals collected from the nylon wire phantom are shown as the functions of depth.

In the case of MOCGCS and CGS, the RF signals were compressed using a match filtering technique prior the envelope detection.

In Fig. 5, the SLL versus depth is shown for different excitation signals. A comparison of the SLL for MOCGCS and CGS shows the efficiency of matched filtering (i.e., the extraction of echoes corresponding to different MOCGCS pairs from the received signal) at various depths. The SLL for the short pulse was also estimated for comparison.

As shown in Fig. 5, the SLL for all types of transmitted signals increases with depth.

In Fig. 6, the SNR determined from the beamformed RF signal along scanline #65, which coincides with the central column of point scatterers of the tissue-mimicking phantom (see Fig. 7), is shown for the short pulse (Fig. 6a), the MOCGCS (Fig. 6b), and the conventional CGS (Fig. 6c) transmission. The SNR was determined as the ratio of the average signal power to the RMS noise power at different depths. The average signal power was estimated for echo samples in 1.5 mm windows corresponding to 5 wavelengths (the wavelength is approximately 0.3 mm). The center of

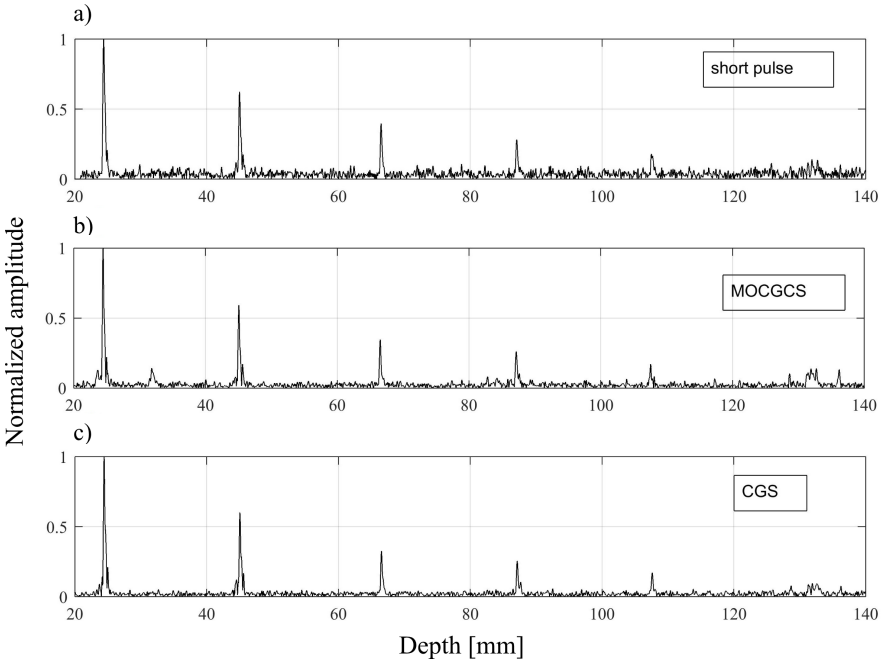

Fig. 4. Envelopes of the processed RF echoes from the nylon wire phantom obtained using: a) the short pulse; b) MOCGCS; c) CGS transmitted signals.

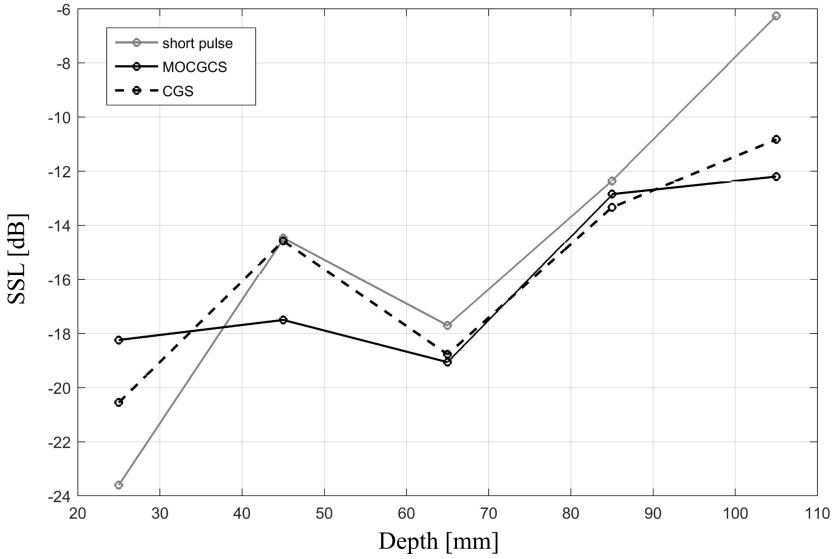

Fig. 5. The SLL vs. depth for the processed signals obtained from the wire phantom (see Fig. 4).

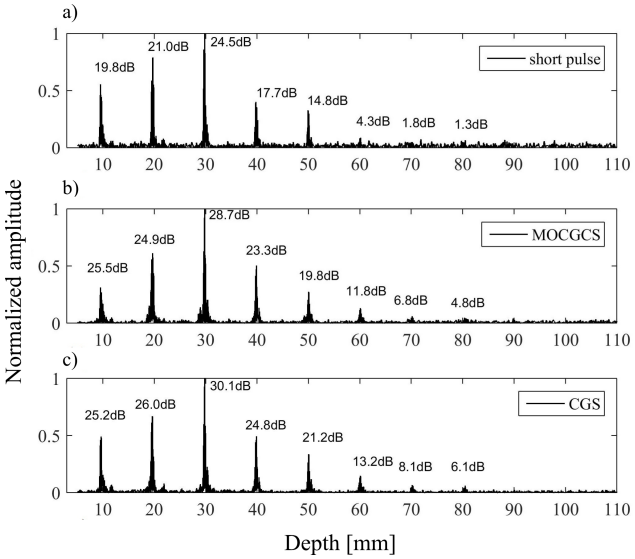

Fig. 6. The SNR for the beamformed RF signal along scanline #65 obtained from the tissue- mimicking phantom using: a) the short pulse; b) MOCGCS; c) conventional CGS transmission. The transmitted voltage was 1.6 V. The absolute values of the beamformed signals are shown.

each window coincided with the peak of echo amplitude at a given depth (corresponding to the wire's location). The RMS noise power was computed for echo samples in a 10 mm (about 34 wavelengths) window starting from 100 mm were only noise is present and the signal component can be neglected (see Fig. 6).

To demonstrate the advantage of the encoded transmission in detecting deeper located wires due to better SNR, the peak-to-peak transmitted voltage was chosen to be 1.6 V, and the measurements were performed without amplifying the detected echoes. As shown in Fig. 6, there is only a slight decrease in the SNR values (not exceeding 1.5 dB across the entire depth range) for MOCGCS compared to CGS transmitted signals was observed. In contrast, the corresponding decrease in the SNR value for the short pulse signal varied from about 5 dB to 8.9 dB across the entire depth range.

In Fig. 7, B-mode images of the tissue-mimicking phantom obtained using the STA image reconstruction method with MOCGCS excitation signals, the conventional STA method with CGS, and short pulse excitation are shown.

The extension of the point spread function for MOCGCS and CGS signals in the axial direction can be observed in Fig. 6. This is due to the SLL increase resulting from the compression of corresponding echo signals. The increase in SLL is primarily influenced by the transducer bandwidth and the non-ideal shape of the generated transmitter sequences (see Fig. 2b through Fig. 2e) as well as the scattering properties of the phantom material, which are similar to those of the real biological tissue.

Finally, the B-mode images of the tissue-mimicking phantom obtained using the STA image reconstruction method with MOCGCS excitation signals, as discussed in (Trots *et al.*, 2022), and the conventional STA method with CGS and short pulse excitation signals, shown in Fig. 7.

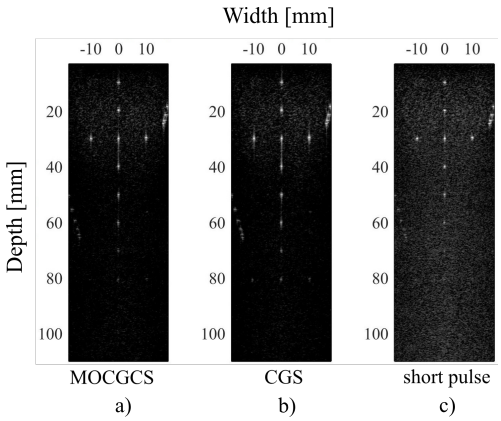

Fig. 7. B-mode images of the tissue-mimicking phantom obtained using the STA image reconstruction method with: a) MOCGCS excitation signals; b) the conventional STA method with CGS; c) short pulse excitation. The transmitted voltage was 1.6 V. All images are displayed on a logarithmic scale with a 40 dB dynamic range.

Figures 8 and 9 show the 2D B-mode reconstructed in-vivo images of the abdominal aorta and common carotid artery from one of the report's authors obtained using MOCGCS, CGS, and short pulse for comparison.

The results of tests for improving sensitivity, increasing the amplitude of received echoes for the three tested transmitter systems, are illustrated in Fig. 10. The received RF echoes were recorded by a single element of the linear array for each transmitted sequence.

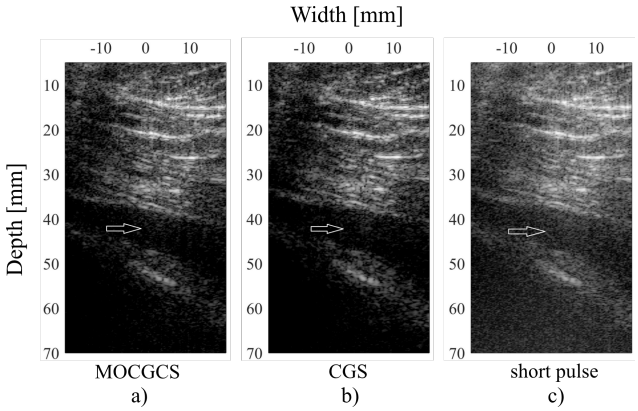

Fig. 8. Comparison of the 2D B-mode images of the abdominal aorta (arrows point to the center of the aorta) obtained in-vivo using: a) MOCGCS; b) CGS; c) short pulse transmission. All images are displayed on a logarithmic scale with a 40 dB dynamic range. The transmitted voltage was 10 V.

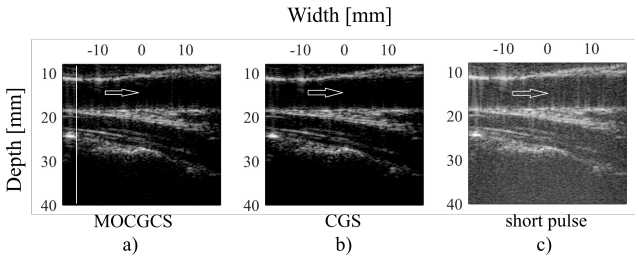

Fig. 9. Comparison of the 2D B-mode images of the common carotid artery (arrows point to the center of the artery) obtained in-vivo: a) using MOCGCS; b) CGS; c) short pulse transmission. All images are displayed on a logarithmic scale with a 40 dB dynamic range. The transmitted voltage was 1.6 V. The vertical line in the leftmost panel indicates the position of the RF echoes shown in Fig. 10.

The recorded echoes were normalized to the maximum value of the CGS signal to show the range of the spanned amplitudes.

The first peaks of the RF signals in Fig. 10 correspond to the signal reflection from the upper wall of the carotid artery at the depth of 10 mm. The amplitude of echoes obtained using the short pulse were at the level of −14.3 dB compared to the coded CGS transmission. In the case of MOCGCS transmission, the decrease in amplitude was about −1.6 dB.

The 2D ultrasound images obtained clearly show that the image resolution is nearly the same in all cases. The reconstruction time for MOCGCS is half that of CGS and the same as that of the short pulse. Using MOCGCS of 4th order or higher can further reduce the reconstruction time, which allows for a proportional increase in frame rate (Huang, 2005). Specifically, in the case of 4th order MOCGCS, a set of four coded sequences is transmitted by four transducers during one transmission, and as a result, four image lines can be constructed after two transmissions.

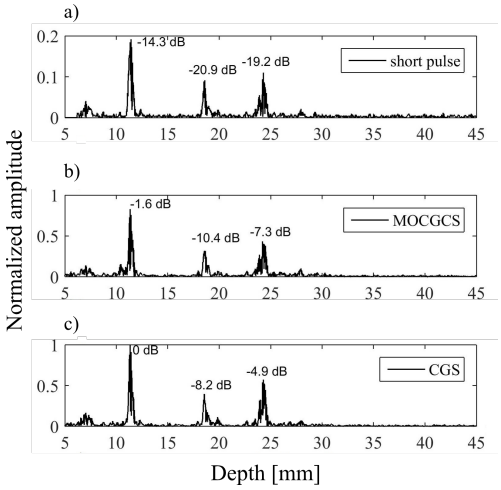

Fig. 10. Normalized magnitudes of the processed RF signals from the human common carotid artery depicted in Fig. 9 for: a) short pulse; b) MOCGCS; c) CGS transmitted signals. The RFs were recorded with element #16 (denoted by the vertical line in the leftmost panel in Fig. 9) during transmission #8 of the STA data acquisition.

4. Conclusions

This study investigated the feasibility of using a set of two complementary Golay sequences (MOCGCS) in ultrasound diagnostics. MOCGCS offers advantages over conventional CGS by enabling faster data acquisition and image reconstruction without compromising image quality. To evaluate MOCGCS performance, the parameters of recorded RF signals acquired from an ideal reflector using MOCGCS, CGS, and short pulse excitation were compared. These parameters included axial resolution that was estimated using the half-maximum duration (−6 dB level) of the signal envelopes (Fig. 4). MOCGCS exhibited minimal (5.8 %) degradation in axial resolution compared to CGS. Despite a slight increase in spatial duration (0.52 mm vs. 0.49 mm for CGS), MOCGCS maintained performance close to CGS. Short pulse excitation displayed a more significant (11 %) decrease in axial resolution compared to CGS, with a spatial duration of 0.55 mm.

The SLL of echoes acquired from a custom-made wire phantom was estimated from their envelopes (Fig. 4) and illustrated against depth (Fig. 5). As expected, a consistent trend of increasing SLL with depth is observed for all signals. The observed increase in SLL with depth can be attributed to growing attenuation of the signal as the two-way propagation path increases and frequency- dependent attenuation acting as a low-pass filter, suppressing higher frequency components of the temporal spectrum. This leads to broadening of the signal in time domain, and the SLL increases. Figure 5 shows that MOCGCS and CGS received signals had very similar SLL values except at a depth of 45 mm, where a difference of about 3 dB was observed

between MOCGCS and CGS SSL values. On the other hand, the SLL of the short pulse signal was about 5 dB higher at a depth of 25 mm and about 4.5 dB lower at a depth of 105 mm compared to the MOCGCS SLL values at specified depths.

SNR values for MOCGCS, CGS and short pulse transmitted signals were compared using RF echoes from the tissue-mimicking phantom. Specifically, SNR at different depths were determined from the beamformed RF signal along scanline #65 of the synthesized B-mode images of the (see Fig. 7). It can be seen from Fig. 6 that SNR values obtained using MOCGCS and CGS signals did not differ significantly. The maximum deterioration of SNR for MOCGCS was observed at depths of 40 mm, close to 1.5 dB. Moreover, coded transmission yielded an increase in SNR ranging from 4.8 dB to 8.9 dB over the short pulse signal across entire range of depths, with this gain becoming especially pronounced for deeper wires located at depths above 40 mm.

Finally, the experimental data from the tissue-mimicking phantom indicated the benefits of MOCGCS. Specifically, B-mode images obtained using the STA method with CGS, MOCGCS, and the short pulse excitation signals are shown in the Fig. 7. It can be seen (by visual assessment) that the images of comparable quality can be obtained using conventional CGS signal and MOGCS, with the latter yielding a twofold frame increase in comparison to the conventional CGS, while maintaining better visualization depth in comparison to the short pulse transmit signal at the same time.

In-vivo recorded scans from the abdominal aorta and common carotid artery of a volunteer seem to be identical regarding minor fragments in backscattered echoes. However, the signal gain was clearly obtained and was proportional to the ratio of the code length to the short pulse length, being close to eight time greater.

The results confirmed that simultaneous MOCGCS transmission and separation of combined RF echoes on the receiver side does not degrade signal parameters compared to conventional CGS. Additionally, transmitting two MOCGCS sets maintains the axial resolution and data acquisition speed of short pulse transmission. The frame rate can potentially be further increased by using more than two MOCGCS sets. The results demonstrate the advantage of MOCGCS in modern ultrasonography compared to conventional short pulse excitation and CGS.

References

1. Bae M.H. (2003), *Ultrasound imaging method and apparatus using orthogonal Golay codes*, U.S. Patent 6638227B2.
2. Bae M.-H., Lee W.-Y, Jeong M.-K., Kwon S.-J. (2002), Orthogonal Golay code based ultrasonic imaging without reducing frame rate, [in:] *2002 IEEE Ultrasonics Symposium, 2002. Proceedings*, pp. 1705–1708, doi: 10.1109/ULTSYM.2002.1192625.
3. Chiao R.Y., Thomas L.J. (2000), Synthetic transmit aperture imaging using orthogonal Golay coded excitation, [in:] *2000 IEEE Ultrasonics Symposium. Proceedings. An International Symposium*, pp. 1677–1680, doi: 10.1109/ULTSYM.2000.921644.
4. Demi L., Viti J., Kusters L., Guidi F., Tortoli P., Mischi M. (2013), Implementation of parallel transmit beamforming using orthogonal frequency division multiplexing-achievable resolution and interbeam interference, *IEEE Transactions on Ultrasonics, Ferroelectrics, and Frequency Control*, **60**(11): 2310–2320, doi: 10.1109/TUFFC.2013.6644735.
5. Golay M.J.E. (1961), Complementary series, *IRE Transactions on Information Theory*, **7**(2): 82–87.
6. Gran F., Jensen J.A. (2006), Frequency division transmission imaging and synthetic aperture reconstruction, *IEEE Transactions on Ultrasonics, Ferroelectrics, and Frequency Control*, **53**(5): 900–911, doi: 10.1109/tuffc.2006.1632681.
7. Huang X. (2005), Simple implementation of mutually orthogonal complementary sets of sequences, [in:] *Proceedings. International Symposium on Intelligent Signal Processing and Communication Systems*, pp. 369–372.
8. Kim B.-H., Song T.-K. (2003), Multiple transmit focusing using modified orthogonal Golay codes for small scale systems, [in:] *IEEE Symposium on Ultrasonics*, pp. 1574–1577, doi: 10.1109/ULTSYM.2003.1293208.
9. Kumru Y., Koymen H. (2018), Beam coding with orthogonal complementary Golay codes for signal-to-noise ratio improvement in ultrasound mammography, *The Journal of the Acoustical Society of America*, **144**(3): 1888–1888, doi: 10.1121/1.5068277.
10. Misaridis T. (2001), *Ultrasound imaging using coded signals*, Ph.D. Thesis, Center for Fast Ultrasound Imaging Technical University of Denmark.
11. Misaridis T., Jensen J.A. (2005), Use of modulated excitation signals in medical ultrasound. Part I: basic concepts and expected benefits, *IEEE Transactions on Ultrasonics, Ferroelectrics, and Frequency Control*, **52**(2): 177–191, doi: 10.1109/TUFFC.2005.1406545.
12. Nowicki A., Secomski W., Litniewski J., Trots I. (2003), On the application of signal compression using Golay's codes sequences in ultrasound diagnostic, *Archives of Acoustics*, **28**(4): 313–324.
13. Peng H., Han X., Lu J. (2006), Study on application of complementary Golay code into high frame rate ultrasonic imaging system, *Ultrasonics*, **44**: e93–e96, doi: 10.1016/j.ultras.2006.06.030.
14. Ramalli A., Guidi F., Boni E., Tortoli P. (2015), A real-time chirp-coded imaging system with tissue attenuation compensation, *Ultrasonics*, **60**: 65–75, doi: 10.1016/j.ultras.2015.02.013.
15. Tian L., Lu X., Xu C., Li Y. (2021), New mutually orthogonal complementary sets with non-power-of-two

lengths, *IEEE Signal Processing Letters*, **28**: 359–363, doi: 10.1109/LSP.2021.3054565.

16. Tseng C.C., Liu C.L. (1972), Complementary sets of sequences, *IEEE Transactions on Information Theory*, **18**(5): 644–652, doi: 10.1109/TIT.1972.1054860.
17. Trots I. (2015), Mutually orthogonal Golay complementary sequences in synthetic aperture imaging systems, *Archives of Acoustics*, **40**(2): 283–289, doi: 10.1515/aoa-2015-0031.
18. Trots I., Nowicki A., Secomski W., Litniewski J. (2004), Golay sequences – side-lobe – canceling codes for ultrasonography, *Archives of Acoustics*, **29**(1): 87–97.
19. Trots I., Tasinkevych Y., Nowicki A. (2015), Orthogonal Golay codes with local beam pattern correction in ultrasonic imaging, *IEEE Signal Processing Letters*, **22**(10): 1681–1684, doi: 10.1109/LSP.2015.2423619.
20. Trots I., Tasinkevych Y., Nowicki A., Lewandowski M. (2011), Golay coded sequences in synthetic aperture imaging systems, *Archives of Acoustics*, **36**(4): 913–926, doi: 10.2478/v10168-011-0061-5.
21. Trots I., Żołek N., Tasinkevych J., Wójcik J. (2022), Mutually Orthogonal Golay Complementary Sequences in Medical Ultrasound Diagnostics. Experimental Study, *Archives of Acoustics*, **47**(3), 399–405, doi: 10.24425/aoa.2022.142013.
22. Wu SW., Chen CY., Liu Z. (2020), How to construct mutually orthogonal complementary sets with non-power-of two lengths?, *IEEE Transactions on Information Theory*, **67**(6): 3464–3472, doi: 10.1109/TIT.2020.2980818.
23. Zhao F., Luo J. (2018), Diverging wave compounding with spatio-temporal encoding using orthogonal Golay pairs for high frame rate imaging, *Ultrasonics*, **89**: 155–165, doi: 10.1016/j.ultras.2018.05.009.